MOL PHARM

MONNA, a Potent and Selective Blocker for Transmembrane Protein with Unknown Function 16/Anoctamin-1[S]

Soo-Jin Oh, Seok Jin Hwang, Jonghoon Jung, Kuai Yu, Jeongyeon Kim, Jung Yoon Choi, H. Criss Hartzell, Eun Joo Roh, and C. Justin Lee

Center for Neuroscience and Center for Functional Connectomics, Brain Science Institute (S.-J.O., J.J., J.K., J.Y.C., C.J.L.), and Chemical Kinomics Research Center, Future Convergence Research Division (S.J.H., E.J.R.), Korea Institute of Science and Technology (KIST), Seoul, Korea; Neuroscience Program, University of Science and Technology, Daejeon, Korea (C.J.L.); KU-KIST Graduate School of Converging Science and Technology, Korea University, Seoul, Korea (C.J.L.); and Department of Cell Biology, Emory University School of Medicine, Atlanta, Georgia (K.Y., H.C.H.)

MOLECULAR PHARMACOLOGY

ABSTRACT

Transmembrane protein with unknown function 16/anoctamin-1 (ANO1) is a protein widely expressed in mammalian tissues, and it has the properties of the classic calcium-activated chloride channel (CaCC). This protein has been implicated in numerous major physiological functions. However, the lack of effective and selective blockers has hindered a detailed study of the physiological functions of this channel. In this study, we have developed a potent and selective blocker for endogenous ANO1 in *Xenopus laevis* oocytes (xANO1) using a drug screening method we previously established (Oh et al., 2008). We have synthesized a number of anthranilic acid derivatives and have determined the correlation between biological activity and the nature and position of substituents in these derived compounds. A structure-activity relationship revealed novel chemical classes of xANO1 blockers. The derivatives contain a $-NO_2$ group on position 5 of a naphthyl group-substituted anthranilic acid, and they fully blocked xANO1 chloride currents with an $IC_{50} < 10$ μM. The most potent blocker, *N*-((4-methoxy)-2-naphthyl)-5-nitroanthranilic acid (MONNA), had an IC_{50} of 0.08 μM for xANO1. Selectivity tests revealed that other chloride channels such as bestrophin-1, chloride channel protein 2, and cystic fibrosis transmembrane conductance regulator were not appreciably blocked by 10~30 μM MONNA. The potent and selective blockers for ANO1 identified here should permit pharmacological dissection of ANO1/CaCC function and serve as potential candidates for drug therapy of related diseases such as hypertension, cystic fibrosis, bronchitis, asthma, and hyperalgesia.

Introduction

Calcium-activated chloride channels (CaCCs) have been found in a wide range of organisms and tissues. They have fundamental and wide-ranging physiological roles in functions such as epithelial secretion, sensory transduction and adaptation, nociception, regulation of smooth muscle cell contraction and vascular tone, and control of neuronal and cardiac excitability (Hartzell et al., 2005). Therefore, CaCCs are

potential drug targets for diarrhea, asthma, cystic fibrosis, and hypertension (Verkman and Galietta, 2009). CaCCs were first described in the early 1980s, in *Xenopus laevis* oocytes, where they generate the fertilization potential that generates a fast electrical inhibition to prevent polyspermy (Miledi, 1982; Barish, 1983). However, the molecular identity of these channels remained elusive until the transmembrane protein with unknown function 16/anoctamin-1 (ANO1) was identified as a CaCC in 2008 (Caputo et al., 2008; Schroeder et al., 2008; Yang et al., 2008). Since then, ANO1 has rapidly garnered attention, and a number of reports have described the properties and physiological roles of this protein (Huang et al., 2009). Notably, a recent study revealed that ANO1 acts as a heat sensor to detect nociceptive thermal stimuli in sensory neurons and possibly mediate nociception (Cho et al., 2012).

The anoctamin family consists of 10 different protein subtypes. Among them, ANO1 has been the most extensively studied (Huang et al., 2009). ANO1 has very similar properties

ABBREVIATIONS: ANO1, anoctamin-1; CaCC, calcium-activated chloride channel; CFTR, cystic fibrosis transmembrane conductance regulator; CLC2, chloride channel protein 2; cRNA, complementary RNA; DCM, dichloromethane; DIDS, 4,4′-diisothiocyanatostilbene-2,2′-disulfonic acid; DMSO, dimethylsulfoxide; DPC, diphenylamine-2-carboxylic acid; hANO1, human ANO1; HEK293, human embryonic kidney 293; HR-ESI-MS, high-resolution electrospray ionization mass spectrometry; mBest1, mouse bestrophin-1; mCLC2, mouse chloride channel protein 2; MONNA, *N*-((4-methoxy)-2-naphthyl)-5-nitroanthranilic acid; NFA, niflumic acid; NPPB, 5-nitro-2-(3-phenylpropylamino)benzoic acid; 4TFMPA, *N*-(4-trifluoromethylphenyl)anthranilic acid; 4TFP4NA, *N*-(4-trifluorophenyl)-4-nitroanthranilic acid; xANO1, *Xenopus laevis* ANO1.

to endogenous CaCCs that have been observed in many different cells, tissues, and organisms. These properties include low-field-strength anion selectivity, Ca^{2+} sensitivity, voltage dependence, and pharmacological profile. Despite the physiological importance of ANO1, the lack of a potent and selective blocker for this protein has impeded a better understanding of the channel at the molecular, biophysical, and pharmacological level. Currently available blockers for CaCCs, including ANO1, include niflumic acid (NFA), 4,4′-diisothiocyanatostilbene-2,2′-disulfonic acid (DIDS), 5-nitro-2-(3-phenylpropylamino)benzoic acid (NPPB), and mefloquine, all of which must be applied at high concentrations to completely block ANO1. The half-maximal concentrations for inhibition (IC_{50}) of NFA, DIDS, and NPPB are reported to be 37.3, 10.7, and 32.3 μM, respectively (Oh et al., 2008). Furthermore, these blockers are known to cause undesirable side effects and block other channels. For example, NFA and DIDS also block the volume-regulated anion channel in some cell types (Xu et al., 1997; Greenwood and Large, 1998), whereas all three, NFA, DIDS, and NPPB, have a blocking effect on the K^+ channel current (Wang et al., 1997; Greenwood and Leblanc, 2007). In addition, NFA, DIDS, and NPPB cause an elevation of intracellular Ca^{2+} concentration in several cell types, which can elicit other cellular responses (Reinsprecht et al., 1995; Shaw et al., 1995; Schultheiss et al., 2000). More recently, several ANO1 inhibitors, such as dichlorophen, benzbromarone, and hexachlorophene, have been identified with high-throughput screening methods, having IC_{50} values of 5.49, 9.97, and 10.0 μM, respectively (Huang et al., 2012). These compounds showed somewhat improved potency over conventional blockers but still fell short of submicromolar potency. In another high-throughput screening study, an aminophenylthiazole (T16A$_{inh}$-A01; Namkung et al., 2011) was found to have an IC_{50} of around 1 μM, but no selectivity information was available. Thus, because of these issues related to low potency and selectivity, there is a very pressing need for improved ANO1 blockers.

Many attempts have been made to uncover chemical compounds that block the endogenous CaCC in *X. laevis* oocytes. In a previous study, we established an optimized protocol for large-scale drug screening using a two-electrode voltage-clamp recording system to search for better blockers for endogenous CaCCs in *X. laevis* oocytes (Oh et al., 2008), which were revealed to be dominantly mediated by endogenous ANO1 in *X. laevis* oocytes (xANO1) (Yang et al., 2008). In our previous study, we found a structural similarity between commercially available CaCC blockers and *N*-(4-trifluoromethylphenyl)anthranilic acid (4TFMPA), a novel potent blocker for xANO1, with an IC_{50} of 6.0 μM, which was synthesized based on structure-activity relationship analysis. In the present study, using the same screening method, we further examined the blocking effect of synthesized compounds using an in-depth structure-activity relationship analysis to discover new ANO1 blockers that have an IC_{50} less than 1 μM.

Materials and Methods

Preparation of Oocytes

As described previously (Oh et al., 2008), mature stage V and VI oocytes were harvested from adult *X. laevis* females (Xenopus-I, Inc., Dexter, MI) that were maintained in an automated maintenance system (Xenopus System; Aquatic Habitats, Apopoka, FL). All experimental procedures described later were performed in accordance with the Korea Institute of Science and Technology (Seoul, Korea) institutional guidelines for humane animal handling. Animals were anesthetized by cooling with ice. Surgically removed ovarian follicles were treated with 2 mg/ml collagenase type IA at room temperature for 90 minutes in Ca^{2+}-free Barth's solution containing 89 mM NaCl, 1.0 mM KCl, 2.4 mM NaHCO$_3$, 0.82 mM MgSO$_4$, and 10 mM HEPES (pH 7.4). Oocytes were extensively rinsed with normal Barth's solution containing 88 mM NaCl, 1.0 mM KCl, 2.4 mM NaHCO$_3$, 0.82 mM MgSO$_4$, 0.33 mM Ca(NO$_3$)$_2$, 1.41 mM CaCl$_2$, and 5 mM HEPES (pH 7.4); placed in a culture of Barth's solution containing 88 mM NaCl, 1.0 mM KCl, 2.4 mM NaHCO$_3$, 0.82 mM MgSO$_4$, 0.33 mM Ca(NO$_3$)$_2$, 0.91 mM CaCl$_2$, 10 mM HEPES, 10 μg/ml streptomycin, and 10 μg/ml penicillin (pH 7.4); and maintained at 18°C. Oocytes were used ~1–4 days after isolation.

Synthesis

Some anthranilic acid derivatives (compound 4f in Figs. 1 and 2F, and six compounds that are not designated in Fig. 2F) had been previously synthesized and reported (Oh et al., 2008). The other anthranilic acid derivatives were synthesized as described in Fig. 1.

Step A. II, IV, and VIII: Thionyl chloride was added dropwise to a solution of benzoic acid derivative (I, III, and VII) in anhydrous methyl alcohol at 0°C. After this addition, the mixture was stirred at reflux for 8~12 hours. The reaction mixture was basified with 10% sodium bicarbonate, and ethyl acetate was added. The organic layer was dried over anhydrous MgSO$_4$, filtered, and the solvent was evaporated to give the products II, IV, and VIII.

Step B. IX: Triflic anhydride was added dropwise to a solution of 4-trifluoromethyl-2-hydroxybenzoicacid methyl ester (VIII) in pyridine and dichloromethane (DCM). This was stirred at room temperature for 6 hours and acidified by the addition of 1 M HCl$_{(aq)}$. The mixture was extracted with DCM and washed with brine. The organic layer was dried over anhydrous MgSO$_4$, filtered, and the solvent was evaporated. IX was purified by column chromatography. Amine derivatives (compound 2a–q, Supplemental Methods, compound synthesis 2) were prepared by this method, except for the commercially available amines.

Step C. V and X: Buchwald-Hartwig cross-coupling of amine (compound 2a–q, IV) and bromo [1b, II; or triflate (1a, IX)] gave anthanilic acid methyl ester (V, X). Tris (dibenzylideneacetone) dipalladium (0)-chloroform adduct (0.05 eq) and (±)-2,2′-bis(diphenylphosphino)-1,1′-binaphthalene (0.10 eq) in anhydrous toluene (3 ml) were stirred at room temperature for 30 minutes. Then, 2-bromo-*N*-nitrobenzoic acid methyl ester, Cs$_2$CO$_3$ (1.4 eq), and aniline derivative (1.2 eq) were added and stirred at 110–130°C for 5–10 hours. The reaction mixture was filtered through Celite (Yakuri Pure Chemicals Co., LTD, Kyoto, Japan) and concentrated in vacuo. Anthanilic acid methyl ester (V, X) was purified by column chromatography.

Step D. VI: Iodination of bromo (V) gave VI. V, NaI (2 eq), CuI (0.05 eq), and trans-*N,N*′-dimethylcyclohexane-1,2-diamine (0.1 eq) in 1,4-dioxane were stirred at 110°C for 5 days. The reaction mixture was filtered through Celite and concentrated in vacuo. VI was purified by column chromatography.

Step E. 3, 4, 5, 6: Hydrolysis of benzoic acid methyl ester derivative (V, VI, and X) was accomplished by refluxing tetrahydrofuran/methanol (MeOH)/H$_2$O (5:3:2) solution in the presence of lithium hydroxide. The reaction mixture was acidified by the addition of 1 M HCl$_{(aq)}$ then extracted with ethyl acetate and washed with brine. The organic layer was dried over anhydrous MgSO$_4$, filtered, and the solvent was evaporated to give anthranilic acid derivatives (3, 4, 5, and 6; Supplemental Methods, compound synthesis 1).

Representative Examples of Active Compounds

_N_-((3-Methoxy)naphthyl)-5-Nitroanthranilic Acid (5p). The final step yields 94.6% (orange powder). Proton nuclear magnetic resonance spectroscopy [^{1}H-NMR, 400 MHz, dimethylsulfoxide (DMSO)–d_6] δ 10.64 (bs, 1H), 8.97 (d, J = 2.7 Hz, 1H), 8.06 (dd, J = 9.4, 2.6 Hz,
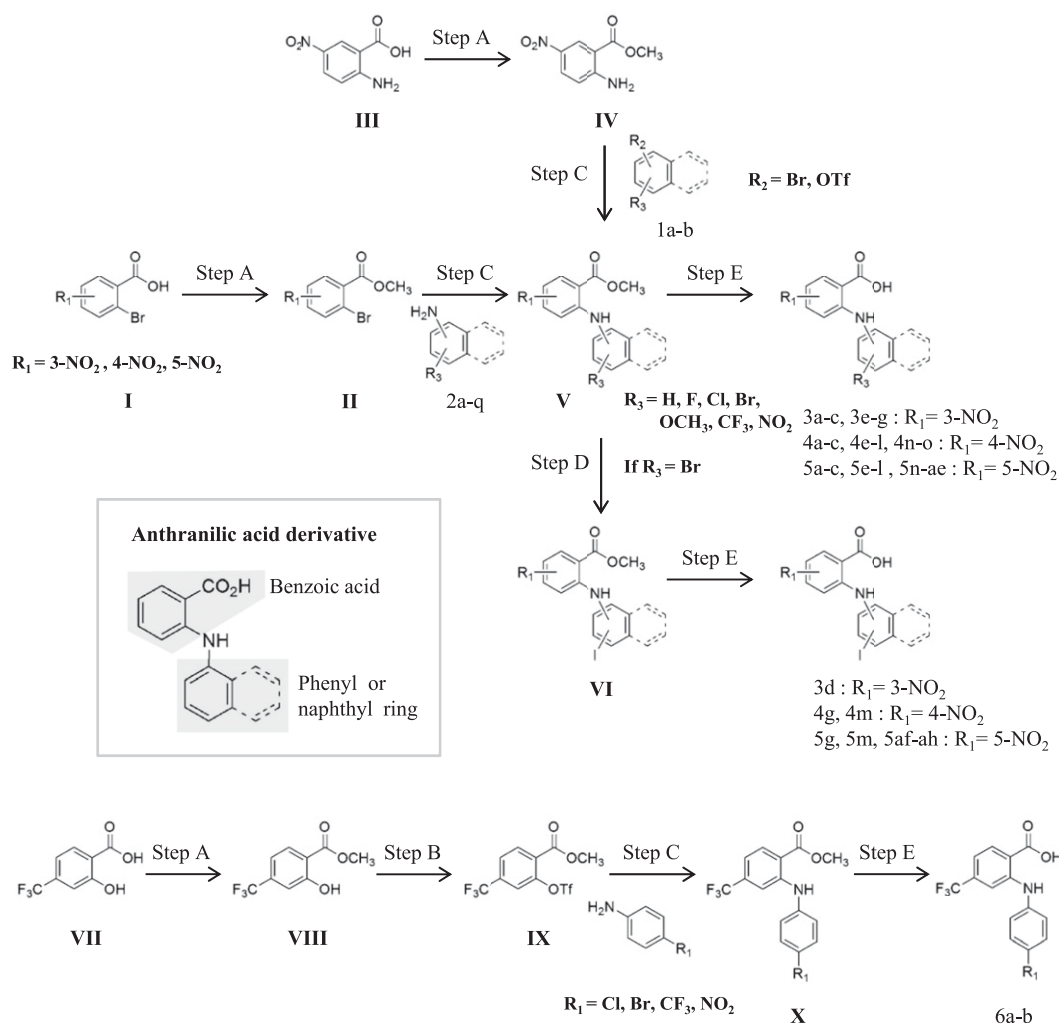
Fig. 1. General synthesis procedures, reagents, and conditions. Step A: trimethylsilyl chloride, MeOH, reflux; step B: OTf$_2$, pyridine, DCM, −78°C to room temperature; step C: 2,2′-bis(diphenylphosphino)-1,1′-naphthyl, Pd$_2$(dba)$_3$ • CHCl$_3$ (tris(dibenzylideneacetone)dipalladium-chloroform adduct), CsCO$_3$, toluene, 110–130°C; step D: CuI, NaI, *trans-N,N′*-dimethylcyclohexane-1,2-diamine, 1,4-dioxane, 110°C; step E: LiOH, tetrahydrofuran/MeOH/H$_2$O (5:3:2), reflux.

1H), 7.84 (d, J = 8.7 Hz, 1H), 7.82 (d, J = 9.3 Hz, 1H), 7.53-7.49 (m, 1H), 7.39-7.35 (m, 1H), 7.19 (d, J = 1.9 Hz, 1H), 7.15 (d, J = 2.3 Hz, 1H), 6.82 (d, J = 9.5 Hz, 1H), 3.91 (s, 3H); ^{13}C-NMR (100 MHz, DMSO–d_6) δ 169.4, 157.5, 154.0, 137.0, 135.8, 129.9, 128.9, 127.7, 125.0, 122.4, 115.7, 114.2, 111.4, 106.0, 55.9; high-resolution electrospray ionization mass spectrometry (HR-ESI-MS) m/z 337.0838 [M–H]$^-$.

N-((6-Methoxy)naphthyl)-5-Nitroanthranilic Acid (5r). The final step yields 90.1% (yellow powder). ^{1}H-NMR (400 MHz, DMSO–d_6) δ 10.65 (bs, 1H), 8.75 (d, J = 2.8 Hz, 1H), 8.09 (dd, J = 9.4, 2.8 Hz, 1H), 7.84 (d, J = 8.0 Hz, 1H), 7.78 (d, J = 9.2 Hz, 1H), 7.56 (dd, J = 7.8, 7.6 Hz, 1H), 7.46 (s, 1H), 7.41 (d, J = 7.2 Hz, 1H), 7.22 (dd, J = 9.0, 2.4 Hz, 1H), 6.66 (d, J = 9.6 Hz, 1H), 3.90 (s, 3H); ^{13}C-NMR (100 MHz, DMSO–d_6) δ 169.4, 158.2, 154.3, 143.5, 136.8, 136.4, 134.5, 129.8, 128.9, 127.2, 126.6, 124.9, 121.3, 120.0, 113.9, 111.2, 107.3, 55.8; HR-ESI-MS m/z 337.0823 [M–H]$^-$.

N-((4-Methoxy)-2-Naphthyl)-5-Nitroanthranilic Acid (5w). The final step yields 98.0% (orange powder). ^{1}H-NMR (400 MHz, DMSO–d_6) δ 10.54 (bs, 1H), 8.74 (d, J = 2.6 Hz, 1H), 8.19 (dd, J = 9.4, 2.5 Hz 1H), 8.11 (d, J = 8.2 Hz, 1H), 7.84 (d, J = 8.0 Hz, 1H), 7.56–7.45 (m, 3H), 7.35 (d, J = 9.4 Hz, 1H), 6.95 (d, J = 9.5 Hz, 1H); ^{13}C-NMR (100 MHz, DMSO–d_6) δ 169.2, 156.6, 152.7, 137.2, 136.7, 134.7, 129.8, 128.9, 127.8, 127.7, 125.5, 123.5, 122.0, 114.4, 113.2, 111.8, 102.8, 56.4; HR-ESI-MS m/z 337.0831 [M–H]$^-$.

N-((7-Methoxy)-2-Naphthyl)-5-Nitroanthranilic Acid (5z). The final step yields 94.9% (yellow powder). ^{1}H-NMR (400 MHz, DMSO–d_6) δ 10.55 (bs, 1H), 8.73 (d, J = 2.8 Hz, 1H), 8.19 (dd, J = 9.4, 2.8 Hz, 1H), 7.91 (d, J = 8.6 Hz, 1H), 7.83 (d, J = 9.0 Hz, 1H), 7.78 (d, J = 1.3 Hz, 1H), 7.32–7.29 (m, 2H), 7.28 (d, J = 9.4 Hz, 1H), 7.14 (dd, J = 8.9, 2.4 Hz, 1H), 3.87(s, 3H)); ^{13}C-NMR (100 MHz, DMSO–d_6) δ 169.2, 158.4, 152.7, 137.2, 136.8, 135.6, 129.8, 129.7, 128.9, 126.8, 121.1, 120.0, 118.7, 114.1, 111.7, 106.2, 55.7; HR-ESI-MS m/z 337.0830 [M–H]$^-$.

N-((8-Methoxy)-2-Naphthyl)-5-Nitroanthranilic Acid (5aa). The final step yields 91.1% (yellow powder). ^{1}H-NMR (400 MHz, DMSO–d_6) 10.56 (bs, 1H), 8.74 (d, J = 2.6 Hz, 1H), 8.20 (dd, J = 9.4, 2.6 Hz, 1H), 8.03 (s, 1H), 7.98 (d, J = 8.6 Hz, 1H), 7.51 (d, J = 8.5 Hz, 1H), 7.43 (dd, J = 7.7, 7.7 Hz, 1H), 7.22 (d, J = 9.4 Hz, 1H), 7.01 (d, J = 7.5 Hz, 1H), 3.97 (s, 3H); ^{13}C-NMR (100 MHz, DMSO–d_6) δ 169.1, 154.8, 152.8, 137.2, 135.8, 132.4, 129.9, 129.8, 128.9, 126.5, 125.8, 124.1, 120.3, 115.3, 113.7, 111.7, 105.6, 56.1; HR-ESI-MS m/z 337.0833 [M–H]$^-$.

N-((4-Bromo)naphthyl)-5-Nitroanthranilic Acid (5ab). The final step yields 97.6% (brown powder). ^{1}H-NMR (400 MHz, DMSO–d_6) 10.72 (bs, 1H), 8.77 (d, J = 2.7 Hz, 1H), 8.24 (d, J = 8.4 Hz, 1H), 8.09 (dd, J = 9.4, 2.8 Hz, 1H), 8.00–7.97 (m, 2H), 7.79 (dd, J = 7.7, 7.3 Hz, 1H), 7.70 (dd, J = 7.7, 7.2 Hz, 1H), 7.55 (d, J = 8.0 Hz, 1H), 6.72 (d, J = 9.4 Hz, 1H); ^{13}C-NMR (100 MHz, DMSO–d_6) 169.3, 153.9, 137.2, 135.0, 132.6, 130.9, 130.6, 129.7, 129.0, 128.8, 128.5, 127.7, 124.4, 123.4, 120.5, 114.1, 111.7; HR-ESI-MS m/z 384.9819 [M–H]$^-$.

***N*-((4-Bromo)-2-Naphthyl)-5-Nitroanthranilic Acid (5ac).** The final step yields 93.5% (yellow powder). ^{1}H-NMR (400 MHz, DMSO–d_6) δ 10.51 (bs, 1H), 8.74 (s, 1H), 8.22 (d, J = 9.8 Hz, 1H), 8.11 (d, J = 8.0 Hz, 1H), 8.00–7.93 (m, 3H), 7.66–7.64 (m, 2H), 7.30 (d, J = 8.8 Hz, 1H); ^{13}C-NMR (100 MHz, DMSO–d_6) δ 168.9, 152.2, 137.7, 136.8, 134.9, 129.8, 129.5, 128.7, 128.2, 127.9, 127.6, 126.6, 123.1, 121.3, 114.4; HR-ESI-MS m/z 384.9839 [M–H]$^-$.

***N*-((7-Bromo)-2-Naphthyl)-5-Nitroanthranilic Acid (5ad).** The final step yields 85% (yellow powder). ^{1}H-NMR (400 MHz, DMSO–d_6) δ 10.64 (bs, 1H), 8.73 (d, J = 2.7, Hz, 1H), 8.20–8.17 (m, 2H), 8.01 (d, J = 8.6 Hz, 1H), 7.89 (d, J = 8.2 Hz, 2H), 7.60–7.58 (m, 1H), 7.53 (dd, J = 8.6, 1.8 Hz, 1H), 7.33 (d, J = 9.4 Hz, 1H); ^{13}C-NMR (100 MHz, DMSO–d_6) δ 169.1, 152.0, 137.5, 135.3, 130.3, 130.0, 129.6, 128.8, 123.9, 120.6, 119.2, 114.0, 112.2; HR-ESI-MS m/z 334.9822 [M–H]$^-$.

***N*-((8-Bromo)-2-Naphthyl)-5-Nitroanthranilic Acid (5ae).** The final step yields 92.4% (yellow powder). ^{1}H-NMR (400 MHz, DMSO–d_6) δ 10.69 (bs, 1H), 8.75 (d, J = 2.8 Hz, 1H), 8.22 (dd, J = 9.4, 2.8 Hz, 1H), 8.09 (d, J = 8.8 Hz, 1H), 8.03 (s, 1H), 8.00 (d, J = 8.2 Hz, 1H), 7.90 (d, J = 7.4 Hz, 1H), 7.62 (dd, J = 8.7, 1.9 Hz, 1H), 7.42 (d, J = 7.8, 7.8 Hz, 1H), 7.33 (d, J = 9.4 Hz, 1H); ^{13}C-NMR (100 MHz, DMSO–d_6) δ 169.0, 152.1, 138.4, 137.7, 132.5, 132.4, 131.3, 131.0, 129.7, 128.8, 128.6, 126.7, 124.5, 121.4, 119.0, 114.1, 112.6; HR-ESI-MS m/z 384.9837 [M–H]$^-$.

***N*-((4-Iodo)naphthyl)-5-Nitroanthranilic Acid (5af).** The final step yields 83.3% (yellow powder). ^{1}H-NMR (400 MHz, DMSO–d_6) δ 10.70 (bs, 1H), 8.76 (s, 1H), 8.22 (d, J = 7.7 Hz, 1H), 8.09 (dd, J = 8.0, 7.7 Hz, 2H), 7.91 (d, J = 8.2 Hz, 1H), 7.74 (dd, J = 7.6, 6.9 Hz, 1H), 7.65 (dd, J = 7.3, 7.2 Hz, 1H), 7.39 (d, J = 7.7 Hz, 1H), 6.72 (d, J = 9.3 Hz, 1H); ^{13}C-NMR (100 MHz, DMSO–d_6) δ 169.3, 153.9, 137.9, 137.2, 135.9, 135.2, 132.8, 130.5, 129.7, 129.3, 128.8, 128.5, 124.9, 123.4, 114.2, 111.8, 98.1; HR-ESI-MS m/z 432.9682 [M–H]$^-$.

***N*-((4-Iodo)-2-Naphthyl)-5-Nitroanthranilic Acid (5ag).** The final step yields 95.3% (yellow powder). ^{1}H-NMR (400 MHz, DMSO–d_6) δ 10.53 (bs, 1H), 8.74 (bs, 1H), 8.21 (d, J = 8.0 Hz, 1H), 8.13 (bs, 1H), 8.00 (bs, 2H), 7.91 (d, J = 5.9 Hz, 1H), 7.62 (bs, 2H), 7.28 (d, J = 8.8 Hz, 1H); ^{13}C-NMR (100 MHz, DMSO–d_6) δ 169.0, 152.4, 137.6, 137.1, 134.9, 134.7, 134.2, 132.2, 131.6, 129.8, 128.9, 128.8, 128.2, 114.4, 112.4, 101.1; HR-ESI-MS m/z 432.9653 [M–H]$^-$.

***N*-((7-Iodo)-2-Naphthyl)-5-Nitroanthranilic Acid (5ah).** The final step yields 96.2% (yellow powder). ^{1}H-NMR (400 MHz, DMSO–d_6) δ 10.93 (bs, 1H), 8.75 (bs, 1H), 8.37 (bs, 1H), 8.18 (d, J = 6.7 Hz, 1H), 7.99 (d, J = 8.5 Hz, 1H), 7.86 (bs, 1H), 7.74 (bs, 2H), 7.51 (d, J = 8.0 Hz, 1H), 7.34 (d, J = 8.6 Hz, 1H); ^{13}C-NMR (100 MHz, DMSO–d_6) δ 169.1, 152.2, 137.5, 137.2, 136.1, 135.8, 134.2, 130.1, 130.0, 129.9, 128.8, 124.2, 119.3, 114.2, 112.4, 93.8; HR-ESI-MS m/z 432.9686 [M–H]$^-$. ^{1}H- and ^{13}C-NMR spectra were recorded on a spectrometer operating at Bruker (Billerica, MA) 400 and 100 MHz, respectively. HR-ESI-MS was carried out by the Advanced Analysis Center at the Korea Institute of Science and Technology.

Electrophysiology of *X. laevis* Oocytes

To test the blocking effect of compounds on xANO1, xANO1 was activated by permeabilizing the plasma membrane to Ca^{2+} and changing the extracellular Ca^{2+} concentration. The oocyte plasma membrane was made permeable to Ca^{2+} by treatment with the Ca^{2+} ionophore ionomycin. Ca^{2+} sequestration by intracellular stores was inhibited with thapsigargin. Oocytes were incubated in an oocyte recording solution containing 96 mM NaCl, 2 mM KCl, 2 mM MgCl$_2$, 0.5 mM EGTA, and 10 mM HEPES (pH 7.4), as well as 10 μM ionomycin, for a 30-minute period. After 30 minutes, the ionomycin was removed from the external solution by washing with oocyte recording solution. Ionomycin-treated oocytes were subsequently incubated in the oocyte recording solution containing 1 μM thapsigargin for 90 minutes. Thapsigargin was then also removed by washing with the oocyte recording solution. Two-electrode voltage-clamp recordings were made using the Warner model OC725B two-electrode voltage clamp amplifier (Warner Instruments, Inc., Hamden, CT) with 1 M KCl-filled microelectrodes (1B150F-4; World Precision Instruments, Sarasota, FL) pulled with a P-97 programmable pipette puller (Sutter Instrument Co., Novato, CA). Microelectrodes had resistances of ~1–3 MΩ. During recordings, oocytes were continuously perfused with oocyte recording solution. All recordings were obtained at a holding potential of –60 mV. Synthesized drug derivatives were prepared in separate bottles and applied by gravity. The flow of solutions was approximately 1 ml/min.

Electrophysiology of Cultured Astrocytes, Human Embryonic Kidney 293 Cells

Mouse astrocyte cell cultures were prepared as previously described (Park et al., 2009). Human embryonic kidney 293 (HEK293) cells were transfected with cDNA [human ANO1 (hANO1), mouse ANO1, or mouse chloride channel protein 2 (mCLC2)] expression plasmids tagged with enhanced green fluorescent protein using Effectene (Qiagen, Valencia, CA) or a blend of lipids (Fugene-6; Roche Molecular Biochemicals, Indianapolis, IN) at 1 μg of DNA per 35-mm culture dish. Single cells identified by enhanced green fluorescent protein fluorescence were used for whole-cell patch clamp experiments within 72 hours. Transfected HEK293 cells were recorded using a conventional whole-cell and an excised inside-out patch clamp. Fire-polished borosilicate glass patch pipettes were ~3–5 MΩ. Experiments were conducted at room temperature (~20–25°C). To activate the channels directly, cultured astrocytes or HEK293 cells were patch clamped with a high Ca^{2+} intracellular solution that contained 146 mM CsCl, 5 mM Ca^{2+}/EGTA/N-methyl-D-glucamine, 2 mM MgCl$_2$, 8 mM HEPES, and 10 mM sucrose, at pH 7.3, adjusted with N-methyl-D-glucamine. The free Ca^{2+} concentration was estimated to be 4.5 μM (Hartzell et al., 2005). The extracellular solution contained the following: 150 mM NaCl, 10 mM HEPES, 3 mM KCl, 2 mM CaCl$_2$, 2 mM MgCl$_2$, and 5.5 mM glucose or 140 mM NaCl, 5 mM KCl, 2 mM CaCl$_2$, 1 mM MgCl$_2$, 15 mM glucose, and 10 mM HEPES at pH 7.3 adjusted with NaOH (300–320 mOsm). Current-voltage curves were established by applying 500-millisecond duration voltage ramps from –100 to +100 mV. Data were acquired with an Axopatch 200A amplifier controlled by Clampex 10.0 software via a Digidata 1322A data acquisition system (Molecular Devices, Sunnyvale, CA). Mouse bestrophin-1 (mBest1) current or hANO1 current was recorded after treatment with N-((4-methoxy)-2-naphthyl)-5-nitroanthranilic acid (MONNA) for 10 minutes. Cells were ruptured and calcium-induced currents were recorded in the presence of MONNA. Current amplitude at one time point of 100–300 seconds after rupture was selected to be analyzed.

Chemicals

Chemical compounds, including the following reagents, were purchased from Sigma-Aldrich (St. Louis, MO): collagenase type 1A, ionomycin-Ca^{2+} salt, thapsigargin, and chelerythrine. HEPES was obtained from J. T. Baker (Mallinckrodt Baker, Inc., Phillipsburg, NJ).

Data Analysis

Currents were digitally recorded with AxoScope software (Axon Instruments, Burlingame, CA) and Clampex 10.0 software. Data analysis was performed with SigmaPlot 10.0 (Systat Software, Inc., San Jose, CA). All current responses elicited during application of a blocker were normalized to the average of a Ca^{2+}-induced Cl$^-$ current applied before application of the blocker. Normalized and average data were fitted using the SigmaPlot three-parameter logistic function to determine the dose-response relationship and the IC$_{50}$. All data are expressed as the mean ± S.E.M. Statistical analyses were performed using a 2-tailed t test.

Results

Potency of Synthesized Derivatives with a Phenyl Group at the B Position. Synthesis of anthranilic acid derivatives was accomplished as described in Fig. 1 (see *Materials and Methods* and Supplemental Methods).

Synthesized and purified compounds were tested for their blocking ability on xANO1 in Ca^{2+} ionophore–treated oocytes using the two-electrode voltage-clamp recording technique as described previously (Oh et al., 2008). We already showed that two repetitive calcium treatments induced currents with almost the same amplitude in our screening system (Oh et al., 2008). We confirmed that four repetitive calcium treatments induce stable currents with similar average amplitude and small variation (Fig. 2, A and B). We expanded our well established recording method to permit simultaneous recording from four oocytes (Fig. 2C). A control ANO1 current in the oocyte was recorded by first adding 5 mM Ca^{2+} to the external bath for 5 seconds. Ca^{2+} was then removed and the drug derivatives added to the zero-Ca^{2+} solution before Ca^{2+} was added to activate ANO1. Current traces were recorded using the four-channel recording system. There was a small variation in peak current amplitudes. In response to repetitive 5-second applications of 5 mM Ca^{2+} plus treatment
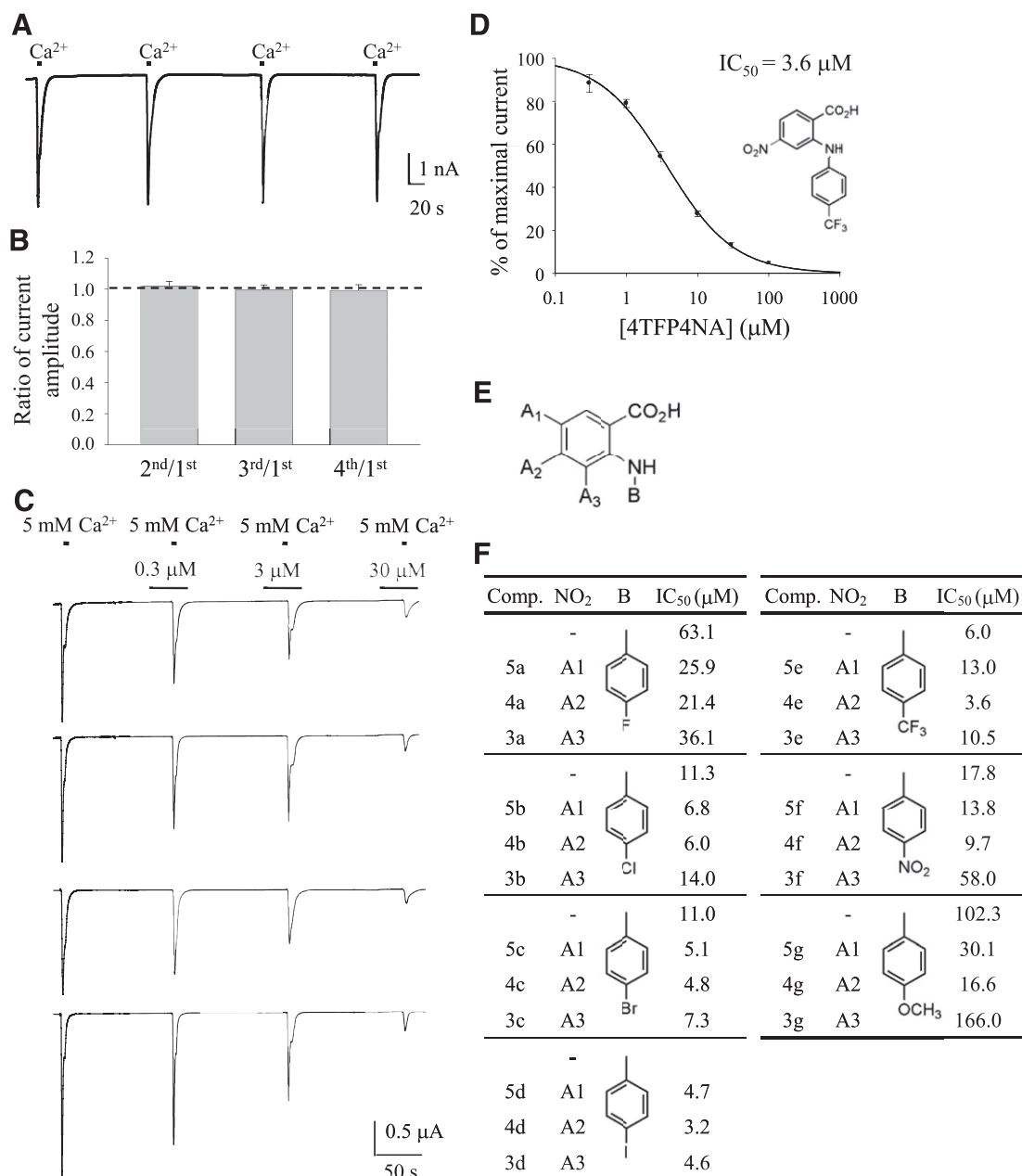

Fig. 2. Potency of synthesized derivatives with a phenyl group at the B position. (A) Representative trace of xANO1 currents induced by four repetitive 5 mM calcium treatments. (B) Summary of the experiments shown in A. Bar graph shows the stable currents with almost the same amplitude induced by four repetitive calcium treatments. Amplitude of the second, third, and fourth currents was normalized by the amplitude of the first current, respectively ($n = 7$). Error bars indicate S.E.M. (C) Representative traces of xANO1 currents by simultaneous four-channel recording before and during application of 4TFP4NA. Oocytes were preincubated with 4TFP4NA for 30 seconds, and currents were induced by 5-second applications of extracellular Ca^{2+}. The currents were measured at –60 mV. (D) Representative dose-response relation of 4TFP4NA block of xANO1 currents ($n = 8$). Error bars indicate S.E.M. (E) Structure of synthesized compound. (F) Summary table for substituents and the IC_{50} of tested compounds. Position A_2 showed the most potent blocking effect. Comp. indicates compounds described in Fig. 1, which shows the synthesis procedures.

with the synthesized compound over the concentration range ($\sim$1–300 μM), peak amplitudes revealed a concentration-dependent block of the xANO1 current, and values for IC_{50} were obtained from dose-response curves. Representative dose-response relation of N-(4-trifluorophenyl)-4-nitroanthranilic acid (4TFP4NA) block of xANO1currents is shown in Fig. 2D.

As we have previously shown that anthranilic acid derivatives with a para-substituted phenyl ring showed the highest blocking potency (Oh et al., 2008), we synthesized various anthranilic acid derivatives with para-positioned substituent groups on the phenyl ring (at position B in Fig. 2E) and with nitro ($-NO_2$) groups positioned at different locations on the benzoic acid ring (at positions A_1–A_3 in Fig. 2E). Figure 2F gives the IC_{50} values of test compounds. Derivative compounds having $-NO_2$ positioned at A_2 on the benzoic acid ring had a relatively high potency in all groups. Substituting different halogen groups on the phenyl ring (position B in Fig. 2E) revealed that potency increased with increasing size of the halogen (I > Br > Cl > F). For substituents with a trifluoromethyl group ($-CF_3$), $-NO_2$, or methoxy group ($-OCH_3$) on the phenyl ring, the most hydrophobic, that with $-CF_3$ was the most potent.

Different Positional Effect Was Observed in Derivatives with Phenyl or Naphthyl Groups at the B Position. As shown in Fig. 2F, the compounds with the greatest potency were produced when $-NO_2$ was located at position A_2 on the benzoic acid ring. We have already verified that 4TFMPA with a $-CF_3$ group para-positioned on the phenyl ring produced a better blocking effect compared with N-(4-nitrophenyl)

anthranilic acid having a $-NO_2$ group located at the same position. Figure 2F shows that the derivative compound having $-CF_3$ on the phenyl ring had a higher potency than the derivative having $-NO_2$ on the phenyl ring. Therefore, we replaced the $-NO_2$ substituent group with $-CF_3$ at position A_2 on the benzoic acid ring (Fig. 3A). However, we found that derivative compounds with $-NO_2$ located at position A_2 on the benzoic acid ring were much more potent than compounds with $-CF_3$ at the same position (Fig. 3B).

Since compounds with more hydrophobic substituent groups had a higher potency in Fig. 2F, we further investigated additional derivative compounds possessing the more hydrophobic naphthyl group at position B (Fig. 3A) in combination with the benzoic acid ring. We synthesized a series of anthranilic acid derivatives having the N-α-naphthyl group. As expected, compounds with a naphthyl group were more potent than compounds with a phenyl group. In contrast to compounds containing the phenyl group, compounds with $-NO_2$ at position A_1 of the benzoic acid ring possessing the naphthyl group were demonstrated to be substantially potent blockers compared with compounds with $-NO_2$ at the A_2 position (Fig. 3C). These data support the idea that a close correlation exists between the potency of blocking xANO1 and the position of substituents on the benzoic acid ring or the hydrophobicity of substituents.

Effect of Substituent Position in the Naphthyl Group on Blocking Potency. As depicted in Fig. 3C, higher potency was observed for derivatives with 4-iodo, 4-bromo, and 4-methoxy substituents on the N-α-naphthyl group. To evaluate the positional effect, all positions on the naphthyl group (Fig. 4A) were substituted with an $-OCH_3$ group. Because it was easier
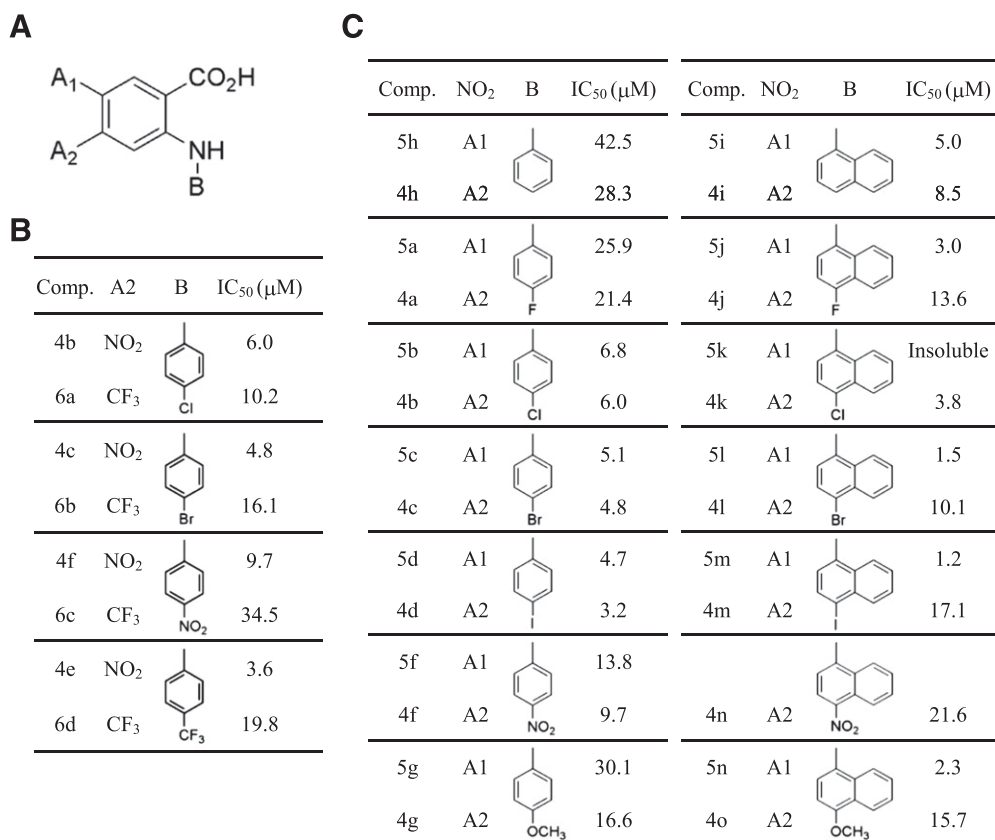
A

B

Comp.	A2	B	IC_{50} (μM)
4b	NO2	(phenyl-Cl)	6.0
6a	CF3		10.2
4c	NO2	(phenyl-Br)	4.8
6b	CF3		16.1
4f	NO2	(phenyl-NO2)	9.7
6c	CF3		34.5
4e	NO2	(phenyl-CF3)	3.6
6d	CF3		19.8

C

Comp.	NO2	B	IC_{50} (μM)	Comp.	NO2	B	IC_{50} (μM)
5h	A1	(phenyl)	42.5	5i	A1	(naphthyl)	5.0
4h	A2		28.3	4i	A2		8.5
5a	A1	(phenyl-F)	25.9	5j	A1	(naphthyl-F)	3.0
4a	A2		21.4	4j	A2		13.6
5b	A1	(phenyl-Cl)	6.8	5k	A1	(naphthyl-Cl)	Insoluble
4b	A2		6.0	4k	A2		3.8
5c	A1	(phenyl-Br)	5.1	5l	A1	(naphthyl-Br)	1.5
4c	A2		4.8	4l	A2		10.1
5d	A1	(phenyl-I)	4.7	5m	A1	(naphthyl-I)	1.2
4d	A2		3.2	4m	A2		17.1
5f	A1	(phenyl-NO2)	13.8				
4f	A2		9.7	4n	A2	(naphthyl-NO2)	21.6
5g	A1	(phenyl-OCH3)	30.1	5n	A1	(naphthyl-OCH3)	2.3
4g	A2		16.6	4o	A2		15.7

Fig. 3. $-NO_2$ at A_2 of benzoic acid ring with phenyl ring-substituted anthranilic acid and $-NO_2$ at A_1 of benzoic acid with naphthyl group-substituted anthranilic acid showed the higher potencies. (A) Structure of synthesized compound. (B) Summary table for substituents and the IC_{50} of tested compounds. $-NO_2$ at position A_2 has a better blocking effect than $-CF_3$. (C) Summary table for substituents and the IC_{50} of tested compounds. $-NO_2$ at position A_2 is best for the phenyl ring, and at position A_1 is best for naphthyl.

to synthesize derivatives with $-OCH_3$ than with iodine $(-I)$, we prepared various compounds with $-OCH_3$ at different positions. Figure 4B shows that all tested compounds conferred a relatively high potency that fully blocked the xANO1 chloride current with an $IC_{50} < 10$ μM. We further synthesized anthranilic acid derivatives with β-naphthyl containing $-OCH_3$ at different positions (Fig. 4C) and examined the blocking effect of these compounds for xANO1 (Fig. 4D). We also synthesized compounds that had bromine $(-Br)$ and $-I$ substituents at positions C_3, C_{10}, C_{13}, or C_{14} (Fig. 4E). These positions were selected because they showed a relatively higher potency with $-OCH_3$. We discovered that anthranilic acid derivatives with the β-naphthyl group with $-OCH_3$ at position C_{10}, with $-I$ at C_{10}, $-Br$ at C_{13}, and $-I$ at C_{13} had a profound blocking effect on xANO1, with IC_{50} values of 0.08, 0.90, 0.22, and 0.55 μM, respectively (Fig. 4E). The most potent blocker found, an anthranilic derivative having β-naphthyl with an $-OCH_3$ group at position C_{10} (N-((4-methoxy)-2-naphthyl)-5-nitroanthranilic acid) and with an IC_{50} of 0.08 μM, was named MONNA.

Validation of Potent Blocker MONNA on the Steady-State Current. In the blocker screening protocol, oocytes were treated with ionomycin to permeabilize the membrane to allow Ca^{2+} influx to activate xANO1. It is possible that the apparent blocking effect could be due to a direct block of ionomycin-mediated Ca^{2+} influx. To confirm that the prominent blocking effect of MONNA occurs at the ionophore or xANO1, we investigated the effect of MONNA on Ba^{2+}- induced currents carried by the ionophore (Fig. 5A). In response to application of Ba^{2+}, a small current mediated by ionomycin was produced. This current was not blocked by MONNA or by 4TFMPA (Fig. 5B).

In our previous study, we showed that Cl^- currents elicited by Ca^{2+} influx in oocytes pemeabilized with ionomycin consisted of a fast peak and a slow steady-state component (Oh et al., 2008). In addition, Schroeder et al. (2008) demonstrated that recording from ionomycin-treated *Axolotl* oocytes injected with xANO1 complementary RNA (cRNA) had calcium-activated currents with both fast and slow components, indicating that both components are mediated by xANO1. To examine whether tested blockers inhibit both the slow steady current as well as the fast current, we changed the test protocol. We measured current amplitudes from the baseline before the treatment of calcium to the steady-state current without MONNA and with MONNA over the concentration range of 1 nM to 100 μM in the presence of calcium (Fig. 5C). Concentration-dependent blocks of ANO1 currents were obtained by measuring the percentage of remaining current, and the IC_{50} was obtained from the dose-response curve (Fig. 5D). Although the IC_{50} for the slow current was slightly different from the IC_{50} for the fast current, MONNA still showed quite a high potency for blocking xANO1 ($IC_{50slow} = 1.0$ μM).

To examine the reversibility of MONNA, we tested the washout of MONNA. Calcium-induced peak current of xANO1 fully recovered after treatment with 0.1 μM MONNA (Fig. 5E). The percentage of current amplitude after MONNA washing over current amplitude before MONNA treatment was 98.2% $\pm$ 3.4% (Fig. 5F).

MONNA Is a Selective Blocker for ANO1. The inhibitory effect of MONNA on other ion channels was evaluated to establish an ion channel selectivity profile for this derivative compound. To verify that MONNA also blocks other members of the ANO1 protein family, inhibitory activity was assessed on hANO1 transiently expressed in HEK293 cells. hANO1 currents were measured by whole-cell patch-clamp recording in the presence of MONNA following 10 minutes of pretreatment with MONNA at a range of concentrations (0.1–10 μM; Fig. 6A). The IC_{50} for MONNA in hANO1 was 1.27 μM, as determined from the dose-response curve by measuring the current amplitude from $+100$ to -100 mV (Fig. 6B). There was no significant difference between the inward current and the outward current of hANO1 in terms of the block percentage (data not shown).
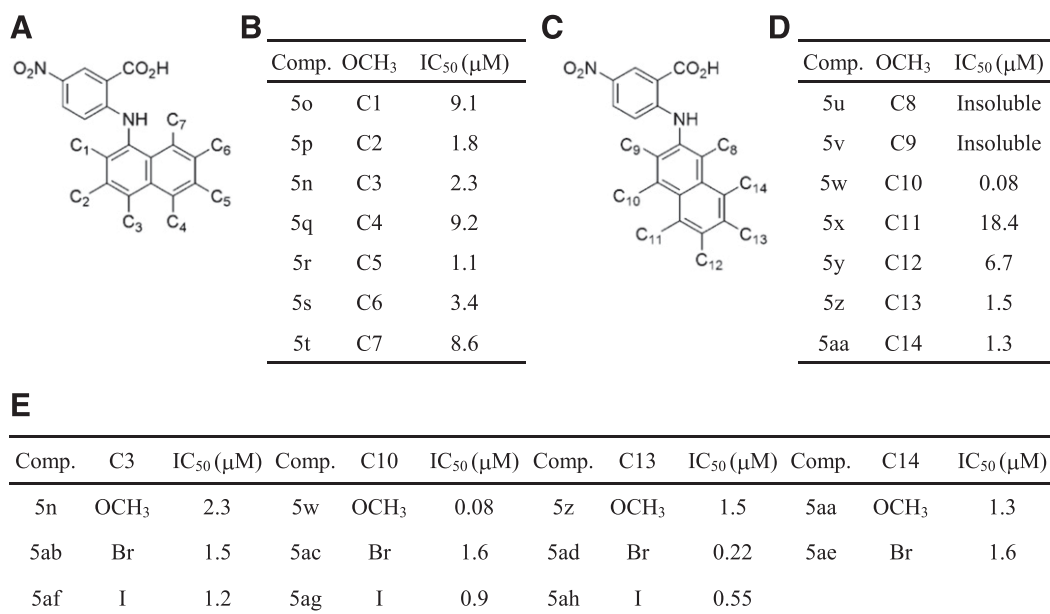

A

B

Comp.	OCH₃	IC₅₀ (μM)
5o	C1	9.1
5p	C2	1.8
5n	C3	2.3
5q	C4	9.2
5r	C5	1.1
5s	C6	3.4
5t	C7	8.6

C

D

Comp.	OCH₃	IC₅₀ (μM)
5u	C8	Insoluble
5v	C9	Insoluble
5w	C10	0.08
5x	C11	18.4
5y	C12	6.7
5z	C13	1.5
5aa	C14	1.3

E

Comp.	C3	IC₅₀ (μM)	Comp.	C10	IC₅₀ (μM)	Comp.	C13	IC₅₀ (μM)	Comp.	C14	IC₅₀ (μM)
5n	OCH₃	2.3	5w	OCH₃	0.08	5z	OCH₃	1.5	5aa	OCH₃	1.3
5ab	Br	1.5	5ac	Br	1.6	5ad	Br	0.22	5ae	Br	1.6
5af	I	1.2	5ag	I	0.9	5ah	I	0.55			

Fig. 4. Effect of substituent position in the naphthyl group on blocking potency. (A and C) Structure of synthesized compound. (B, D, and E) Summary table for substituents and the IC_{50} of tested compounds. $-OCH_3$ at position C_{10} of β-naphthyl has the most potent blocking effect.
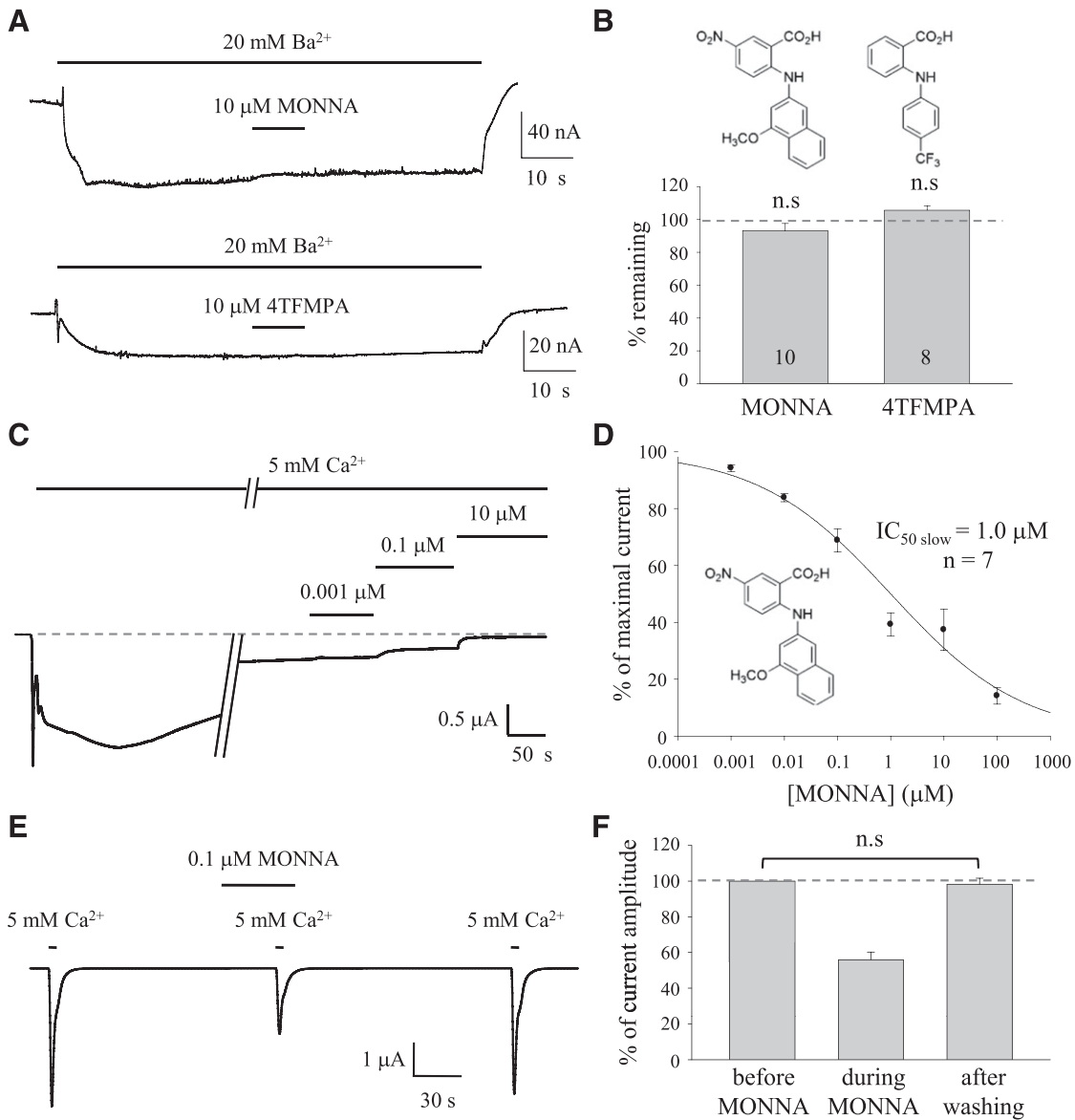
Fig. 5. Validation of potent blocker MONNA on the steady-state current. (A) Representative traces to show blocking of Ba^{2+}-induced currents by MONNA and 4TFMPA in the ionophore. The current was measured at –60 mV. (B) Structure of tested compounds and summary bar graph of the experiments shown in A. Each number in the bar indicates the number of cells tested. Error bars indicate S.E.M. (C) Representative traces for test blocking effect of MONNA on the slow steady current component. A dashed line indicates the baseline. Current amplitudes were measured from baseline before the treatment of calcium to the steady-state current without MONNA and with MONNA over the concentration range in the presence of calcium. (D) IC_{50} and dose-response relation of MONNA for the slow current component of the Ca^{2+}-activated Cl^- current. Concentration-dependent block of ANO1 currents was obtained by measuring the percentage of remaining current, and IC_{50} was obtained from the dose-response curves. (E) Representative trace to show the washout of MONNA. A total of 0.1 μM MONNA was fully washed out after a 100-second wash with recording solution. (F) Summary bar graph of percentage current amplitude measured from the experiments shown in E (n = 9). Error bars indicate S.E.M. n.s., no significant statistical difference with the 2-tailed t test.

We further examined the blocking effect of MONNA on other chloride channels such as bestrophin-1, CLC2, and cystic fibrosis transmembrane conductance regulator (CFTR). For mBest1, endogenously expressed in cultured mouse cortical astrocytes (Fig. 6D; Park et al., 2009, currents were recorded in the whole-cell patch-clamp mode with 4.5 μM Ca^{2+} in the patch pipette. MONNA (30 μM) was treated 10 minutes before and during patching. HEK293 cells transiently transfected with cDNA of human bestrophin-1 or mouse CLC2 (mCLC2) were recorded with the whole-cell patch-clamp technique. HEK293

cells were held at 0 mV and stimulated with voltage steps ranging from –100 to +100 mV. Current amplitudes were collected before and 2 minutes after the application of 10 μM MONNA. CFTR currents induced by isoproterenol were recorded with the two-electrode voltage-clamp method in *X. laevis* oocytes coinjected with cRNA encoding human CFTR and the β-adrenergic receptor. The oocytes were held at –60 mV, and 10 μM MONNA was added to the isoproterenol-containing solution (Fig. 6C). No significant blocking effect was observed with current responses in the presence of 30 μM MONNA for
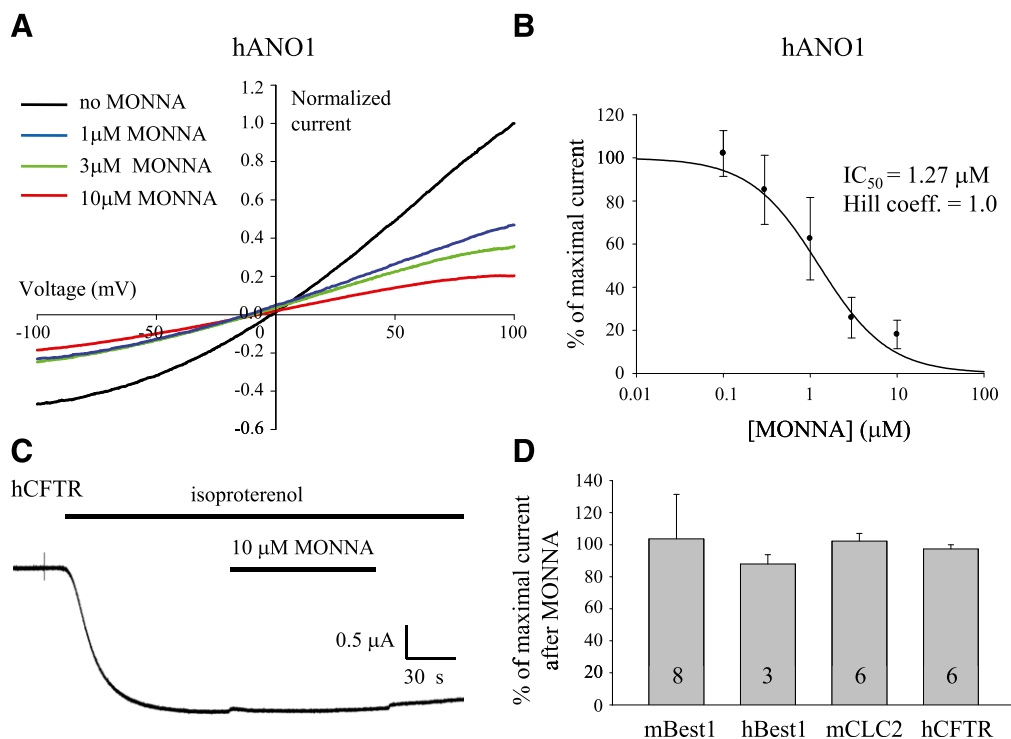
Fig. 6. MONNA is a selective blocker for ANO1. (A) Representative I–V response of HEK293 cells expressing hANO1 under the whole-cell patch-clamp configuration, with 4.5 μM Ca^{2+} in the patch pipette. Each current trace was normalized to the current measured at +100 mV. (B) IC_{50} and dose-response relation of MONNA for hANO1 ($n = \sim$3–12). (C) Representative trace to show the effect of MONNA on the human CFTR (hCFTR) currents induced by treatment with 10 μM isoproterenol in voltage-clamped *X. laevis* oocytes expressing hCFTR and the β-adrenergic receptor. (D) Bar graph to show the blocking effect of MONNA on other chloride channels. Responses to various chloride channels were evaluated in cultured mouse cortical astrocytes expressing endogenous mBest1, in transiently transfected HEK293 cells expressing human bestrophin-1 (hBest1) or mCLC2, or in *X. laevis* oocytes stably expressing hCFTR, in the absence or presence of MONNA. Thirty micromolars MONNA was applied to cells expressing mBest1, and 10 μM MONNA was applied to hBest1, mCLC2, and hCFTR. Each number in the bar indicates the number of cells tested. Error bars indicate S.E.M.

mBest1 and 10 μM MONNA for human bestrophin-1, mCLC2, and human CFTR (Fig. 6D).

Discussion

In this study, we have identified a novel class of ANO1 blocker that inhibits the endogenous ANO1 in *X. laevis* oocytes (xANO1), highlighting anthranilic acid derivatives with β-naphthyl possessing the substituent group $-OCH_3$, $-I$, or $-Br$. Notably, MONNA, an anthranilic derivative having β-naphthyl with an $-OCH_3$ group at C_{10}, is the most potent and selective blocker for xANO1 with an IC_{50} of 0.08 μM.

Our drug screening method proved to be extremely efficient compared with the general blind screening for ion channel blockers. We validated the potent ANO1 blocker MONNA with less than 100 synthesized compounds. We were able to take advantage of target structure-focused libraries based on an anthranilic acid scaffold with specific substituents to arrive at the desired compounds because we began with a lead compound that was an ANO1 blocker. Therefore, fewer compounds required screening to obtain hit compounds. This strategy meant a smaller-scale, higher-quality screening process and dramatically reduced the subsequent hit-to-lead timescale.

Currently available blockers for ANO1 must be applied in high concentrations to completely block ANO1 and are not very selective. Many attempts have been made to discover blockers for CaCCs. In particular, recent reports have focused on the high-throughput screening of small molecules that inhibit the activity of ANO1 (Namkung et al., 2011; Huang

et al., 2012). Although these recently screened small-molecule blockers have a high potency for ANO1 compared with conventional known blockers, the selectivity profile of these blockers should be determined.

The gating of ANO1 and the endogenous CaCC in oocytes is enigmatic and not completely understood (Kuruma and Hartzell, 2000; Xiao et al., 2011). However, all available evidence suggests that calcium-activated fast and slow currents are mediated by the same channel. Schroeder et al. (2008) showed that recording from ionomycin-treated *Axolotl* oocytes injected with xANO1 cRNA had calcium-activated currents which had both fast and slow components. These two components with two distinct kinetics mediated by the xANO1 channel are probably associated with different conformational states; the fast current is the open state and the slow current may be a desensitized state. The conformational states of ion channels are believed to affect the affinity and efficacy of agonists and blockers. State-dependent affinity of ion channel blocker is a well-known phenomenon. Therefore, we can predict that different IC_{50} values of MONNA to the fast and slow currents of xANO1 come from the differential conformational states.

The profile of this new compound MONNA, as a selective blocker of ANO1, is very intriguing. MONNA strongly blocked chloride currents in xANO1 as well as in hANO1, suggesting a common blocking effect of MONNA in other members of the ANO1 protein family. The level of sensitivity in endogenous xANO1 was different from that of hANO1 expressed in HEK cells. In our previous report, we confirmed that untransfected HEK293 cells showed negligible Ca^{2+}-induced current response

(Park et al., 2009). Therefore, the difference in sensitivity for MONNA between endogenous xANO1 and hANO1 is not because of anion channel expression in HEK293 cells. Rather, differences in IC$_{50}$ of MONNA between xANO1 and hANO1 possibly come from the conformational state or sequence or splice variant differences. To measure the blocking effect of MONNA on hANO1, current amplitude at one time point of 100–300 seconds after rupture was selected to be analyzed. We can predict that the conformational state of hANO1 is close to the desensitized state at this time point. Consistent with this idea, the IC$_{50}$ of hANO1 (1.27 μM) is not significantly different from the IC$_{50slow}$ of xANO1 (1.0 μM). The other possibility is the quantitative difference in pharmacology between overexpressed ANO1 and native CaCCs as previously reported (Oh et al., 2008; Yang et al., 2008). The concentration-current response from ANO1 channels overexpressed in HEK cells suggests a near complete block of currents by 10 μM NFA, DIDS, and NPPB (Yang et al., 2008), whereas NFA, DIDS, and NPPB showed far less sensitivity to endogenous xANO1, with IC$_{50}$ values of 37.3, 10.7, and 32.3 μM, respectively, using our screening method (Oh et al., 2008). This is probably due to the molecular diversity within the ANO1 family or splice variants of ANO1 which reflect the pharmacological diversity of the CaCC. Although whole-cell CaCC currents are superficially similar in different cell types, including *X. laevis* oocytes, various secretory epithelial cells, hepatocytes, vascular, airway, and gut smooth muscle cells, Jurkat T cells, and pulmonary artery endothelial cells, there are significant differences in the pharmacology of these currents and their splice variants (Hartzell et al., 2005). Future studies to better understand the variable pharmacology of Cl$^-$ channel-blocking drugs may include a determination of the specific expression of different members of the ANO1 family and ANO1 splice variants.

From our current results, we are unable to distinguish whether the site of compound action on ANO1 is external or internal. However, a previous study revealed that diphenylamine-2-carboxylic acid (DPC) blocked from the outside and NFA blocked from both the inside and the outside when recordings were made in excised inside-out and outside-out patches from *X. laevis* oocytes (Qu and Hartzell, 2001). There is a possibility that blocking of NFA from the inside involves NFA crossing the membrane to block from the outside. Because the molecular structure of MONNA is similar to that of DPC and NFA, we can predict that MONNA might also block xANO1 in a manner that is similar to DPC or NFA. There is a possibility that MONNA can bind to the calcium binding site of ANO1 from the inside of the cells and influence the calcium dependence of ANO1. The crystal structure of ANO1 is not fully known, but when such structural information becomes available, the drug discovery process should be significantly accelerated. Meanwhile, the availability of a selective blocker for ANO1 should be beneficial for further understanding of the function of ANO1 and for possible therapeutic applications in those diseases associated with ANO1.

Authorship Contributions

Participated in research design: Oh, Hwang, Hartzell, Roh, Lee.
Conducted experiments: Oh, Hwang, Jung, Yu, Kim, Choi.

Contributed new reagents or analytic tools: Oh, Hwang, Jung, Roh.
Performed data analysis: Oh, Hwang, Jung, Yu, Kim, Hartzell, Roh, Lee.
Wrote or contributed to the writing of the manuscript: Oh, Hwang, Yu, Hartzell, Roh, Lee.

References

Barish ME (1983) A transient calcium-dependent chloride current in the immature Xenopus oocyte. *J Physiol* **342**:309–325.
Caputo A, Caci E, Ferrera L, Pedemonte N, Barsanti C, Sondo E, Pfeffer U, Ravazzolo R, Zegarra-Moran O, and Galietta LJ (2008) TMEM16A, a membrane protein associated with calcium-dependent chloride channel activity. *Science* **322**:590–594.
Cho H, Yang YD, Lee J, Lee B, Kim T, Jang Y, Back SK, Na HS, Harfe BD, and Wang F et al. (2012) The calcium-activated chloride channel anoctamin 1 acts as a heat sensor in nociceptive neurons. *Nat Neurosci* **15**:1015–1021.
Greenwood IA and Large WA (1998) Properties of a Cl- current activated by cell swelling in rabbit portal vein vascular smooth muscle cells. *Am J Physiol* **275**:H1524–H1532.
Greenwood IA and Leblanc N (2007) Overlapping pharmacology of Ca2+-activated Cl- and K+ channels. *Trends Pharmacol Sci* **28**:1–5.
Hartzell C, Putzier I, and Arreola J (2005) Calcium-activated chloride channels. *Annu Rev Physiol* **67**:719–758.
Huang F, Rock JR, Harfe BD, Cheng T, Huang X, Jan YN, and Jan LY (2009) Studies on expression and function of the TMEM16A calcium-activated chloride channel. *Proc Natl Acad Sci USA* **106**:21413–21418.
Huang F, Zhang H, Wu M, Yang H, Kudo M, Peters CJ, Woodruff PG, Solberg OD, Donne ML, and Huang X et al. (2012) Calcium-activated chloride channel TMEM16A modulates mucin secretion and airway smooth muscle contraction. *Proc Natl Acad Sci USA* **109**:16354–16359.
Kuruma A and Hartzell HC (2000) Bimodal control of a Ca(2+)-activated Cl(-) channel by different Ca(2+) signals. *J Gen Physiol* **115**:59–80.
Miledi R (1982) A calcium-dependent transient outward current in Xenopus laevis oocytes. *Proc R Soc Lond B Biol Sci* **215**:491–497.
Namkung W, Phuan PW, and Verkman AS (2011) TMEM16A inhibitors reveal TMEM16A as a minor component of calcium-activated chloride channel conductance in airway and intestinal epithelial cells. *J Biol Chem* **286**:2365–2374.
Oh SJ, Park JH, Han S, Lee JK, Roh EJ, and Lee CJ (2008) Development of selective blockers for Ca²(+)-activated Cl channel using Xenopus laevis oocytes with an improved drug screening strategy. *Mol Brain* **1**:14.
Park H, Oh SJ, Han KS, Woo DH, Park H, Mannaioni G, Traynelis SF, and Lee CJ (2009) Bestrophin-1 encodes for the Ca2+-activated anion channel in hippocampal astrocytes. *J Neurosci* **29**:13063–13073.
Qu Z and Hartzell HC (2001) Functional geometry of the permeation pathway of Ca2+-activated Cl-channels inferred from analysis of voltage-dependent block. *J Biol Chem* **276**:18423–18429.
Reinsprecht M, Rohn MH, Spadinger RJ, Pecht I, Schindler H, and Romanin C (1995) Blockade of capacitive Ca2+ influx by Cl- channel blockers inhibits secretion from rat mucosal-type mast cells. *Mol Pharmacol* **47**:1014–1020.
Schroeder BC, Cheng T, Jan YN, and Jan LY (2008) Expression cloning of TMEM16A as a calcium-activated chloride channel subunit. *Cell* **134**:1019–1029.
Schultheiss G, Frings M, Hollingshaus G, and Diener M (2000) Multiple action sites of flufenamate on ion transport across the rat distal colon. *Br J Pharmacol* **130**:875–885.
Shaw T, Lee RJ, and Partridge LD (1995) Action of diphenylamine carboxylate derivatives, a family of non-steroidal anti-inflammatory drugs, on [Ca2+]i and Ca (2+)-activated channels in neurons. *Neurosci Lett* **190**:121–124.
Verkman AS and Galietta LJ (2009) Chloride channels as drug targets. *Nat Rev Drug Discov* **8**:153–171.
Wang HS, Dixon JE, and McKinnon D (1997) Unexpected and differential effects of Cl- channel blockers on the Kv4.3 and Kv4.2 K+ channels. Implications for the study of the I(to2) current. *Circ Res* **81**:711–718.
Xiao Q, Yu K, Perez-Cornejo P, Cui Y, Arreola J, and Hartzell HC (2011) Voltage- and calcium-dependent gating of TMEM16A/Ano1 chloride channels are physically coupled by the first intracellular loop. *Proc Natl Acad Sci USA* **108**:8891–8896.
Xu WX, Kim SJ, So I, Kang TM, Rhee JC, and Kim KW (1997) Volume-sensitive chloride current activated by hyposmotic swelling in antral gastric myocytes of the guinea-pig. *Pflugers Arch* **435**:9–19.
Yang YD, Cho H, Koo JY, Tak MH, Cho Y, Shim WS, Park SP, Lee J, Lee B, and Kim BM et al. (2008) TMEM16A confers receptor-activated calcium-dependent chloride conductance. *Nature* **455**:1210–1215.

Address correspondence to: C. Justin Lee, Center for Neuroscience and Center for Functional Connectomics, Korea Institute of Science and Technology, Seoul, Korea 136-791. E-mail: cjl@kist.re.kr; and Eun Joo Roh, Chemical Kinomics Research Center, Future Convergence Research Division, Korea Institute of Science and Technology, Seoul, Korea 136-791. E-mail: r8636@kist.re.kr